

Topological Yu-Shiba-Rusinov chain in monolayer transition-metal dichalcogenide superconductors

Junhua Zhang and Vivek Aji

Department of Physics & Astronomy, University of California, Riverside, CA 92521, USA

(Dated: October 18, 2018)

Monolayers of transition-metal dichalcogenides (TMDs) are two-dimensional materials whose low energy sector consists of two inequivalent valleys. The valence bands have a large spin splitting due to lack of inversion symmetry and strong spin-orbit coupling. Furthermore the spin is polarized up in one valley and down in the other (in directions perpendicular to the two-dimensional crystal). We focus on lightly hole-doped systems where the Fermi surface consists of two disconnected circles with opposite spins. For both proximity induced and intrinsic local attractive interaction induced superconductivity, a fully gapped intervalley pairing state is favored in this system, which is an equal superposition of the singlet and the $m=0$ triplet for the lack of centrosymmetry. We show that a ferromagnetically ordered magnetic-adatom chain placed on a monolayer TMD superconductor provides a platform to realize one-dimensional topological superconducting state characterized by the presence of Majorana zero modes at its ends. We obtain the topological phase diagram and show that the topological superconducting phase is affected not only by the adatom spacing and the direction of the magnetic moment, but also by the orientation of the chain relative to the crystal.

Introduction.— Monolayers of transition-metal group-VI dichalcogenides (TMDs), MX_2 ($M = \text{Mo, W}$ and $X = \text{S, Se, Te}$), are direct band-gap semiconductors, which have two-dimensional (2D) hexagonal crystal structure [1–4]. Similar to graphene, the low-energy physics involves multiple valleys in momentum space. There are two significant differences from graphene and other graphene-like materials pertinent to the discussion of topological superconductivity. First is the lack of inversion symmetry and second is the existence of a strong spin-orbit coupling (SOC) originating from the d -orbitals of the heavy metal atoms. These result in 1) a large energy gap (~ 1.5 eV) between the conduction and valence bands as opposed to Dirac nodes, and 2) a Zeeman-like spin splitting ($0.15 - 0.5$ eV) of the valence bands, with spins polarized perpendicular to the plane but in opposite directions between upper and lower valence bands and between different valleys. The unique electronic structure of monolayer TMDs, i.e., the spin degrees of freedom are locked with the valley degrees of freedom, has triggered intensive research on this class of 2D materials recently, e.g. a possible platform for spintronics and valleytronics applications [5, 6].

The physics of spin-valley locking characterized by an Ising-type configuration of electron spins in momentum space is maximal in the lightly hole-doped systems. In this regime the Fermi energy crosses the upper valence bands and is well separated from the lower valence bands as shown in Fig. 1(a). The low-energy physics is characterized by disconnected non-degenerate Fermi surfaces (FS's) in different valleys with opposite spin directions, as shown in Fig. 1(b). The superconducting (SC) state in this system has been studied recently [7–11]. The superconductivity, resulting either from a local attractive density-density interaction or from proximity to an s -wave superconductor, is characterized by inter-valley pairing with the Cooper pair being an equal mixture of the singlet and $m=0$ triplet (note that parity is no longer a good quantum number). Since the Cooper-pair partners of opposite spin live on disconnected FS's with spin pinned normal to the plane, dubbed Ising superconductivity, novel properties associated

with the SC state of the system in this new regime are anticipated.

In particular, the recent efforts to search for possible platforms to realize topological superconductivity and Majorana zero modes have identified the need for strong SOC, time reversal breaking and superconductivity. A relevant proposal is that of a magnetic-adatom chain placed on top of an s -wave superconductor with (or effectively with) SOC [12–30]. In this scenario, the topological band arises from hybridizing the Yu-Shiba-Rusinov (YSR) states [31–33] at different impurity sites. However, the previous proposals, either based on helical spin chains [12–20, 27] or on superconductors with Rashba SOC [22, 28], all require a chiral (or effectively chiral) spin texture of the electrons coupled to the magnetic moments. While Ising spin structure lacks chirality, TMDs do possess two essential ingredients to realize one-dimensional (1D) topological superconductivity: (1) an odd-parity component to the order parameter and (2) spin structure of the Cooper pair locked perpendicular to the 2D crystal. As a result, monolayer TMD superconductor, with ferromagnetically ordered magnetic-adatom chain placed on it, has a large phase space for realizing Majorana zero modes making it a possible platform for topological quantum computation [34–40].

In this Rapid Communication, we study a chain of magnetic adatoms placed on the monolayer TMD superconductors, as shown in Fig. 1(c), in which the superconductivity of monolayer TMDs results either from a local attractive density-density interaction or by proximity to an s -wave superconducting substrate, e.g., Nb, NbS₂, etc.. We show that a chain of ferromagnetically ordered magnetic impurities on the monolayer TMD superconductors can induce a topological superconducting phase in the YSR band. To this end, we analytically construct a tight-binding description for the deep YSR bands, i.e., the subgap bands close to the center of the host SC gap, to obtain an effective Hamiltonian and calculate the topological phase diagram. We find that the topological property is affected by the orientation of the chain on the 2D crystal plane and the direction of the magnetic moment.

When the chain is oriented along the arm-chair directions of the hexagonal lattice which correspond to the mirror planes in this material, the odd-parity component vanishes due to the mirror symmetry along these directions, resulting in vanishing topological pairing in the chain. When the magnetic moments of the adatoms point perpendicular to the plane, the topological pairing also vanishes since it is parallel to the characteristic SOC direction in this material. However, for any direction of the magnetic moments with a finite in-plane component and any orientation of the chain other than the specific (three mirror) directions, there exists a large topological phase space in this system as shown in the topological phase diagram.

Superconducting state in monolayer TMDs.— The superconducting state in the lightly hole-doped monolayer TMDs, arising either from a local attractive density-density interaction or from proximity to an s -wave superconductor, is described by the mean-field Hamiltonian ($\hbar = 1$) with superconducting gap Δ

$$\mathcal{H}_{SC}(\mathbf{k}) = \sum_{\tau s} \xi_k d_{\tau s}^\dagger(\mathbf{k}) d_{\tau s}(\mathbf{k}) + \Delta d_{+\uparrow}^\dagger(\mathbf{k}) d_{-\downarrow}^\dagger(-\mathbf{k}) + h.c. \quad (1)$$

where $\xi_k = -k^2/2m - \mu$ is the valence band dispersion at chemical potential μ , $\tau = \pm$ is the valley index and $s = \uparrow, \downarrow$ is the spin index which are in the combinations as $\tau s = +\uparrow, -\downarrow$ due to spin-valley locking in the system. Note that we use \mathbf{k} to represent momentum measured from the corresponding valley center and \mathbf{p} to represent momentum measured from the Brillouin zone (BZ) center. We also take the notation that $d_{\tau s}^\dagger(\mathbf{k})$ ($d_{\tau s}(\mathbf{k})$) creates (annihilates) a quasiparticle with momentum \mathbf{k} and spin s in the valley τ , and $c_s^\dagger(\mathbf{p})$ ($c_s(\mathbf{p})$) creates (annihilates) a quasiparticle with momentum \mathbf{p} and spin s . The Hamiltonian (1) describes a fully gapped superconductor with inter-valley pairing. For convenience, we take the order parameter Δ to be real.

Transforming from the $d_{\tau s}(\mathbf{k})$ basis to the $c_s(\mathbf{p})$ basis, the real-space Green's function for the superconductor, defined in the spin and particle-hole space by choosing the convention for the Nambu spinor as $(c_\uparrow(\mathbf{r}), c_\downarrow(\mathbf{r}), c_\uparrow^\dagger(\mathbf{r}), -c_\downarrow^\dagger(\mathbf{r}))^T$ where $c_s^\dagger(\mathbf{r})$ ($c_s(\mathbf{r})$) is the Fourier transform of $c_s^\dagger(\mathbf{p})$ ($c_s(\mathbf{p})$), has the form

$$\hat{G}(\mathbf{r}, E) = \hat{G}_{\text{even}}(\mathbf{r}, E) + \hat{G}_{\text{odd}}(\mathbf{r}, E), \quad (2)$$

where the subscripts represent spatially even and odd parts with the expressions

$$\hat{G}_{\text{even}}(\mathbf{r}, E) = \frac{1}{2} \left\{ [\mathcal{I}_0^+(\mathbf{r}, E) + \mathcal{I}_0^-(\mathbf{r}, E)] (E + \Delta \hat{\rho}_x) + [\mathcal{I}_1^+(\mathbf{r}, E) + \mathcal{I}_1^-(\mathbf{r}, E)] \hat{\rho}_z \right\}, \quad (3)$$

$$\hat{G}_{\text{odd}}(\mathbf{r}, E) = \frac{1}{2} \left\{ [\mathcal{I}_0^+(\mathbf{r}, E) - \mathcal{I}_0^-(\mathbf{r}, E)] (E + \Delta \hat{\rho}_x) + [\mathcal{I}_1^+(\mathbf{r}, E) - \mathcal{I}_1^-(\mathbf{r}, E)] \hat{\rho}_z \right\} \hat{\sigma}_z. \quad (4)$$

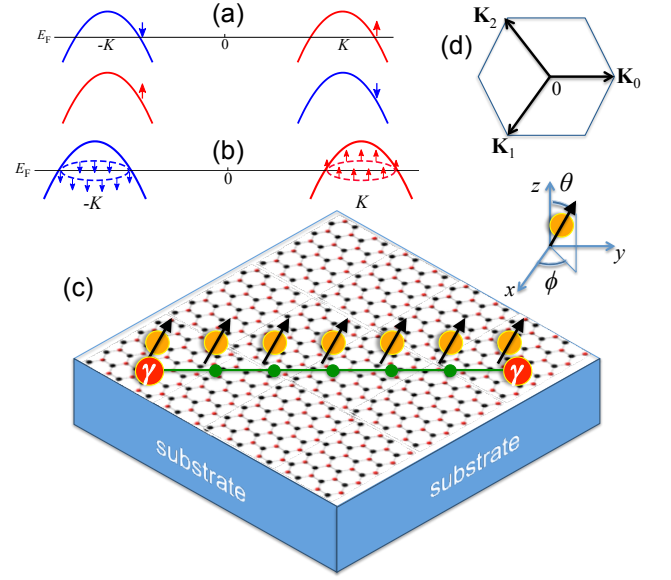


FIG. 1. (Color online) Schematic illustrations of (a) the lightly-hole doped system and (b) its disconnected Fermi surface pieces with opposite spin directions. (c) Schematic setup of the proposed magnetic moments forming a ferromagnetic chain on the monolayer TMD superconductor. We show that Majorana zero modes γ can be realized at the ends of the YSR chain induced by the magnetic moments. (d) Schematic illustration of the three momenta \mathbf{K}_n , $n = 0, 1, 2$, associated with the valley centers.

The Pauli matrices $\hat{\sigma}$'s and $\hat{\rho}$'s operate in spin and particle-hole space, respectively. $\mathcal{I}_0^\pm(\mathbf{r}, E) \equiv \frac{1}{3} \sum_{n=0,1,2} e^{\pm i\mathbf{K}_n \cdot \mathbf{r}} I_0(\mathbf{r}, E)$ and $\mathcal{I}_1^\pm(\mathbf{r}, E) \equiv \frac{1}{3} \sum_{n=0,1,2} e^{\pm i\mathbf{K}_n \cdot \mathbf{r}} I_1(\mathbf{r}, E)$ take an average over the three pairs of valleys centered at momenta (measured from BZ center) $\pm \mathbf{K}_n$, $n = 0, 1, 2$, recovering the three-fold rotational symmetry in the continuum model. Here we choose the direction of \mathbf{K}_0 as the x direction as shown in Fig. 1(d), then $\mathbf{K}_n \cdot \mathbf{r} = Kr \cos(n\frac{2}{3}\pi + \varphi)$, where φ is the angle between \mathbf{r} and \mathbf{K}_0 (the x axis). $I_0(\mathbf{r}, E)$ and $I_1(\mathbf{r}, E)$ are defined as

$$I_0(\mathbf{r}, E) = -\frac{N_F}{2\pi} \int_{-D}^D d\xi \int_{-\pi}^{\pi} d\phi_{\mathbf{k}} \frac{e^{ik(\xi)r \cos \phi_{\mathbf{k}}}}{\xi^2 + \Delta^2 - E^2}, \quad (5)$$

$$I_1(\mathbf{r}, E) = -\frac{N_F}{2\pi} \int_{-D}^D d\xi \int_{-\pi}^{\pi} d\phi_{\mathbf{k}} \frac{e^{ik(\xi)r \cos \phi_{\mathbf{k}}}}{\xi^2 + \Delta^2 - E^2} \xi, \quad (6)$$

where D is an energy cut-off, $\phi_{\mathbf{k}} = \arctan(k_y/k_x)$, $k(\xi) = k_F + \xi/v_F$ with Fermi momentum k_F and Fermi velocity v_F , and N_F is the density of states at the Fermi energy. The analytical results for the above integrals are evaluated in the limit $D \rightarrow \infty$ and are presented in the Supplemental Material. The spatially-odd property of \hat{G}_{odd} is due to the fact that $\mathcal{I}_{0(1)}^\pm(-\mathbf{r}) = \mathcal{I}_{0(1)}^\mp(\mathbf{r})$.

Equation (4) shows that the odd-parity part has a spin structure with a characteristic direction perpendicular to the plane (z direction), originating from the intrinsic SOC. The existence of an odd-parity component with a specific spin struc-

ture is the key to the presence of topological superconductivity, as shown later. When \mathbf{r} is perpendicular to each of the \mathbf{K}_n , $\mathbf{r} \perp \mathbf{K}_n$ $n = 0, 1, 2$, the odd-parity part vanishes. This corresponds to three special directions parallel to the arm-chair edges of the hexagonal lattice about which mirror symmetry is preserved.

Yu-Shiba-Rusinov chain.— We consider a chain of magnetic adatoms placed on superconducting monolayer TMDs. The magnetic moments $\mathbf{S}_j = S(\sin \theta_j \cos \phi_j, \sin \theta_j \sin \phi_j, \cos \theta_j)$ are located at positions \mathbf{R}_j separated by equal spacing a with classical spin S pointing in the direction (θ_j, ϕ_j) as shown in Fig. 1(c). Here we consider a ferromagnetic ordering of the magnetic moments: $\theta_j = \theta$ and $\phi_j = \phi$. The impurity magnetic moment couples to the quasiparticles in the host superconductor through $\mathcal{H}_{imp} = \int d\mathbf{r} \psi^\dagger(\mathbf{r}) \mathcal{H}_{imp}(\mathbf{r}) \psi(\mathbf{r})$ where $\psi(\mathbf{r}) = \begin{pmatrix} c_\uparrow(\mathbf{r}), c_\downarrow(\mathbf{r}), c_\downarrow^\dagger(\mathbf{r}), -c_\uparrow^\dagger(\mathbf{r}) \end{pmatrix}^T$ is the Nambu spinor at position \mathbf{r} , and

$$\mathcal{H}_{imp}(\mathbf{r}) = -J \sum_j \mathbf{S}_j \cdot \hat{\sigma} \delta(\mathbf{r} - \mathbf{R}_j), \quad (7)$$

where J is the exchange coupling ($J > 0$). In order to find the band structure of the chain of YSR states induced by the magnetic impurities, we solve the Schrodinger equation

$$[\mathcal{H}_{SC} + \mathcal{H}_{imp}(\mathbf{r})] \psi(\mathbf{r}) = E \psi(\mathbf{r}). \quad (8)$$

In terms of the Green's function for the superconductor $\hat{G}(\mathbf{p}, E) = [E - \mathcal{H}_{SC}(\mathbf{p})]^{-1}$ and transforming to momentum space, the equation can be rewritten as

$$\psi(\mathbf{p}) = -J \sum_j \hat{G}(\mathbf{p}, E) (\mathbf{S}_j \cdot \hat{\sigma}) e^{-i\mathbf{p} \cdot \mathbf{R}_j} \psi(\mathbf{R}_j). \quad (9)$$

Transforming back to real space and considering the spinor at site i on the left-hand side, the chain equation becomes

$$\psi(\mathbf{R}_i) = -J \sum_j \hat{G}(\mathbf{R}_i - \mathbf{R}_j, E) (\mathbf{S}_j \cdot \hat{\sigma}) \psi(\mathbf{R}_j), \quad (10)$$

where $\hat{G}(\mathbf{R}_i - \mathbf{R}_j, E) = \int \frac{d\mathbf{p}}{(2\pi)^2} e^{i\mathbf{p} \cdot (\mathbf{R}_i - \mathbf{R}_j)} \hat{G}(\mathbf{p}, E)$.

To solve for the bound-state spectrum, separating the on-site and inter-site terms and using the short-hand notation $\psi_i \equiv \psi(\mathbf{R}_i)$, the chain equation takes the form:

$$\hat{M}(E) \psi_i + \sum_{j \neq i} \hat{M}_{ij}(E) \psi_j = 0, \quad (11)$$

with the expressions for the on-site and inter-site matrices

$$\hat{M}(E) = 1 + J \hat{G}(\mathbf{0}, E) (\mathbf{S}_i \cdot \hat{\sigma}), \quad (12)$$

$$\hat{M}_{ij}(E) = J \hat{G}(\mathbf{R}_{ij}, E) (\mathbf{S}_j \cdot \hat{\sigma}), \quad (13)$$

where $\mathbf{R}_{ij} \equiv \mathbf{R}_i - \mathbf{R}_j$ for $j \neq i$, and $\hat{G}(\mathbf{0}, E) = \int \frac{d\mathbf{p}}{(2\pi)^2} \hat{G}(\mathbf{p}, E) = -\pi N_F \frac{E + \Delta \hat{\rho}_x}{\sqrt{\Delta^2 - E^2}}$. The YSR bound state

induced by a single magnetic impurity is determined by $\hat{M}(E) \psi_i = 0$, giving rise to the eigen energies $E_\pm = \pm \Delta \frac{1 - \tilde{J}^2}{1 + \tilde{J}^2}$ in terms of the dimensionless exchange coupling $\tilde{J} \equiv J \pi N_F S$, and the eigen spinors

$$\psi_+ \sim \begin{pmatrix} \chi_\uparrow \\ \chi_\uparrow \end{pmatrix}, \quad \psi_- \sim \begin{pmatrix} \chi_\downarrow \\ -\chi_\downarrow \end{pmatrix}, \quad (14)$$

$$\chi_\uparrow = \begin{pmatrix} \cos \frac{\theta}{2} \\ e^{i\phi} \sin \frac{\theta}{2} \end{pmatrix}, \quad \chi_\downarrow = \begin{pmatrix} e^{-i\phi} \sin \frac{\theta}{2} \\ -\cos \frac{\theta}{2} \end{pmatrix}, \quad (15)$$

up to a normalization constant. These eigen spinors ψ_\pm are used as local basis when deriving the effective Hamiltonian for the YSR chain.

Tight-binding description.— To analytically construct a tight-binding description for the YSR chain [17, 22, 28], we take the deep and shallow band approximations: Consider the YSR band is close to the center of the host gap, i.e., $\tilde{J} \sim 1$, and its bandwidth is small compared to the host gap, i.e., $E \ll \Delta$, which requires a large spacing a between the adatoms. In these approximations, we linearize $\hat{M}(E)$ with respect to E : $\hat{M}(E) \approx \hat{M}_0 - \hat{M}_1 \cdot E$, and set $E \rightarrow 0$ in the inter-site matrix $\hat{M}_{ij}(E \rightarrow 0)$. Then the tight-binding description is given by

$$\sum_j \hat{H}_{ij} \psi_j = E \psi_i \quad (16)$$

with the on-site and inter-site operators being $\hat{H}_{ii} = \hat{M}_1^{-1} \hat{M}_0$ and $\hat{H}_{ij} = \hat{M}_1^{-1} \hat{M}_{ij}(E \rightarrow 0)$, $j \neq i$, respectively. The explicit expressions for \hat{M}_0 , \hat{M}_1 , and $\hat{M}_{ij}(E \rightarrow 0)$ are given in the Supplemental Material.

Effective BdG Hamiltonian.— By projecting \hat{H}_{ij} onto the local YSR basis $(\psi_+, \psi_-)^T$, we obtain the effective Bogoliubov-de Gennes (BdG) Hamiltonian as

$$H_{\text{eff}}(i, j) = \begin{bmatrix} h_{\text{eff}}(\mathbf{R}_{ij}) + b_{\text{eff}}(\mathbf{R}_{ij}) & \Delta_{\text{eff}}(\mathbf{R}_{ij}) \\ \Delta_{\text{eff}}^*(\mathbf{R}_{ji}) & -h_{\text{eff}}(\mathbf{R}_{ij}) + b_{\text{eff}}(\mathbf{R}_{ij}) \end{bmatrix}, \quad (17)$$

where

$$h_{\text{eff}}(\mathbf{R}_{ij}) = \epsilon_0 \delta_{ij} + \frac{1}{2\tilde{J}} J S \Delta^2 [\mathcal{I}_0^+(\mathbf{R}_{ij}) + \mathcal{I}_0^-(\mathbf{R}_{ij})], \quad (18)$$

$$b_{\text{eff}}(\mathbf{R}_{ij}) = \frac{1}{2\tilde{J}} J S \Delta^2 [\mathcal{I}_0^+(\mathbf{R}_{ij}) - \mathcal{I}_0^-(\mathbf{R}_{ij})] \cos \theta, \quad (19)$$

$$\Delta_{\text{eff}}(\mathbf{R}_{ij}) = \frac{-1}{2\tilde{J}} J S \Delta [\mathcal{I}_1^+(\mathbf{R}_{ij}) - \mathcal{I}_1^-(\mathbf{R}_{ij})] e^{-i\phi} \sin \theta, \quad (20)$$

with the on-site energy $\epsilon_0 = \Delta(1 - \tilde{J})/\tilde{J}$, i.e., the effective chemical potential of the YSR band. For $\tilde{J} \sim 1$, $\epsilon_0 \sim 0$, the YSR band is close to the center of the host gap. Here the integrals $\mathcal{I}_{0(1)}^\pm$ are evaluated for $E \rightarrow 0$ and considered vanishing for $i = j$.

The effective pairing term has the spatial property: $\Delta_{\text{eff}}(-\mathbf{R}_{ij}) = -\Delta_{\text{eff}}(\mathbf{R}_{ij})$, since it is arising from the odd-parity component \hat{G}_{odd} of the bulk superconductor. This describes a p -wave pairing of the spinless fermions in 1D, reminiscent of the Kitaev chain [41], despite the long-range nature of the inter-site hopping and pairing. Clearly, when the magnetic moments point perpendicular to the plane (in z direction), $\theta = 0, \pi$, the effective pairing vanishes indicating that the subgap band is not superconducting in this case. However, as long as the magnetic moment has a finite in-plane component, the subgap band can become superconducting. Besides the even-parity hopping $h_{\text{eff}}(\mathbf{R}_{ij})$, we also observe that a polarization component along the z axis induces an odd-parity inter-site term $b_{\text{eff}}(\mathbf{R}_{ij})$. Its presence is also due to the odd-parity component \hat{G}_{odd} in the bulk superconductor. $b_{\text{eff}}(\mathbf{R}_{ij})$ is analogous to the response to an applied magnetic field.

Topological superconducting phase.— To study the topological property, transforming the BdG Hamiltonian to momentum space, we obtain

$$H_{\text{eff}}(p) = \begin{bmatrix} h_{\text{eff}}(p) + b_{\text{eff}}(p) & \Delta_{\text{eff}}(p) \\ \Delta_{\text{eff}}^*(p) & -h_{\text{eff}}(p) + b_{\text{eff}}(p) \end{bmatrix}. \quad (21)$$

The details are given in the Supplemental Material. The Hamiltonian is in the symmetry class D [42–44], and thus is characterized by the Z_2 topological invariant \mathcal{M} [41]:

$$\mathcal{M} = \text{sgn}[h_{\text{eff}}(0)h_{\text{eff}}(\pi/a)]. \quad (22)$$

The system is in the topological superconducting phase when $\mathcal{M} = -1$, whereas $\mathcal{M} = +1$ indicates a non topological phase. We obtain the topological phase diagram by calculating \mathcal{M} .

The topological phase is affected by the direction of the magnetic moments as indicated in Eq. (20). A finite topological gap requires the magnetic moments deviate from z direction and reaches its maximum when the moments lie in the plane. This is achieved experimentally by aligning the moments using magnetic field before cooling the system. The topological property is also affected by the orientation of the chain, characterized by the angle φ_c between the chain and the x direction in the crystal plane, as shown in Fig. 2(a). As discussed before, the inter-site coupling (13) through $\hat{G}(\mathbf{r}, E)$ involves phase factors: $\mathbf{K}_n \cdot \mathbf{r} = Kr \cos(n\frac{2}{3}\pi + \varphi_c)$ for \mathbf{r} on the chain. When $\mathbf{r} \perp \mathbf{K}_n$ ($n = 0, 1, 2$), corresponding to the three arm-chair directions in the hexagonal lattice as indicated by the dashed lines in Fig. 2(a), $\Delta_{\text{eff}}(\mathbf{R}_{ij})$ vanishes due to the vanishing odd-parity component \hat{G}_{odd} in the bulk superconductor. These special directions are related to the mirror planes in the system. A finite topological gap requires the chain orientation to avoid these special directions. The phase diagram calculated using the Z_2 topological invariant \mathcal{M} is valid between two mirror planes, e.g., $\varphi_c \in (-\pi/6, \pi/6)$ and is symmetric with respect to each mirror plane, as well as having threefold rotational symmetry. Furthermore, it is symmetric for φ_c and $-\varphi_c$. Therefore, the calculation for the

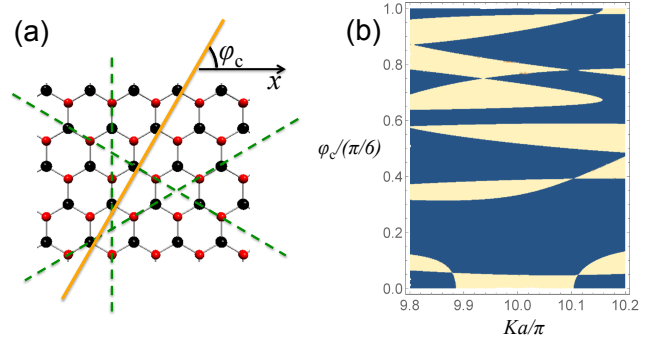


FIG. 2. (Color online) (a) Schematic illustration of the chain orientation relative to the 2D crystal structure characterized by the angle φ_c . The dashed lines correspond to the mirror-plane directions along which the YSR bands are gapless. (b) Calculated topological phase diagram for the effective Hamiltonian (21) as a function of $\varphi_c \in (0, \pi/6)$ and Ka ($K = |\mathbf{K}_n|$) for the magnetic moments aligning in the crystal plane, i.e., $\theta = \pi/2$. Here we take $\tilde{J} = 1$ such that $\epsilon_0 = 0$. The dark color ($\mathcal{M} = -1$) represents the topological phase characterized by an odd number of Majoranas at its ends, whereas the light color ($\mathcal{M} = +1$) refers to the non-topological phase.

regime $\varphi_c \in (0, \pi/6)$ is sufficient as other sectors are related through symmetry. The adatom spacing a is another factor affecting the topological property because the band structure of the YSR chain is sensitive to it.

Figure 2(b) shows the calculated topological phase diagram for the effective Hamiltonian (21) as a function of φ_c and Ka ($K = |\mathbf{K}_n|$) for the magnetic moments aligning in the crystal plane $\theta = \pi/2$. Here we take $\tilde{J} = 1$ such that the effective chemical potential is right in the middle of the bulk gap. The dark color represents the topological phase characterized by an odd number of Majoranas at its ends, whereas the light color refers to the non-topological phase. We can see that there is a large parameter space in which the chain is expected to be in a topological phase.

Conclusions.— In conclusion we have investigated the topological nature of a ferromagnetic adatom chain proximally coupled to an inter-valley paired TMD superconductor. Strong SOC and the lack of inversion symmetry in monolayer TMDs can support a topological superconducting state in the YSR chain, as long as the chain is not oriented along mirror planes of the 2D crystal and the magnetic moments have a finite in-plane component. Thus, for a large parameter regime, Majorana bound states at the end of the chain can be realized, providing a new platform to explore topological phases of matter.

Acknowledgements.— This work is supported by ARO W911NF1510079.

Notes added.— Recently, we became aware of a preprint [45] with similar conclusions.

-
- [1] K. S. Novoselov, D. Jiang, F. Schedin, T. J. Booth, V. V. Khotkevich, S. V. Morozov, and A. K. Geim, *Proc. Natl. Acad. Sci. U.S.A.* **102**, 10451 (2005), <http://www.pnas.org/content/102/30/10451.full.pdf>.
- [2] A. Splendiani, L. Sun, Y. Zhang, T. Li, J. Kim, C.-Y. Chim, G. Galli, and F. Wang, *Nano Letters* **10**, 1271 (2010), pMID: 20229981, <http://dx.doi.org/10.1021/nl903868w>.
- [3] K. F. Mak, C. Lee, J. Hone, J. Shan, and T. F. Heinz, *Phys. Rev. Lett.* **105**, 136805 (2010).
- [4] B. Radisavljevic, A. Radenovic, J. Brivio, V. Giacometti, and A. Kis, *Nature Nanotechnology* **6**, 147 (2011).
- [5] D. Xiao, G.-B. Liu, W. Feng, X. Xu, and W. Yao, *Phys. Rev. Lett.* **108**, 196802 (2012).
- [6] K. F. Mak, K. L. McGill, J. Park, and P. L. McEuen, *Science* **344**, 1489 (2014), <https://www.sciencemag.org/content/344/6191/1489.full.pdf>.
- [7] J. M. Lu, O. Zheliuk, I. Leermakers, N. F. Q. Yuan, U. Zeitler, K. T. Law, and J. T. Ye, *Science* **350**, 1353 (2015), <http://science.sciencemag.org/content/350/6266/1353.full.pdf>.
- [8] Y. Saito, Y. Nakamura, M. S. Bahramy, Y. Kohama, J. Ye, Y. Kasahara, Y. Nakagawa, M. Onga, M. Tokunaga, T. Nojima, Y. Yanase, and Y. Iwasa, *Nature Physics* **12**, 144 (2016), [arXiv:1506.04146 \[cond-mat.supr-con\]](https://arxiv.org/abs/1506.04146).
- [9] X. Xi, Z. Wang, W. Zhao, J.-H. Park, K. T. Law, H. Berger, L. Forró, J. Shan, and K. F. Mak, *Nature Physics* **12**, 139 (2016), [arXiv:1507.08731 \[cond-mat.supr-con\]](https://arxiv.org/abs/1507.08731).
- [10] B. T. Zhou, N. F. Q. Yuan, H.-L. Jiang, and K. T. Law, *Phys. Rev. B* **93**, 180501 (2016).
- [11] E. Sosenko, J. Zhang, and V. Aji, *ArXiv e-prints* (2015), [arXiv:1512.01261 \[cond-mat.supr-con\]](https://arxiv.org/abs/1512.01261).
- [12] T.-P. Choy, J. M. Edge, A. R. Akhmerov, and C. W. J. Beenakker, *Phys. Rev. B* **84**, 195442 (2011).
- [13] S. Nadj-Perge, I. K. Drozdov, B. A. Bernevig, and A. Yazdani, *Phys. Rev. B* **88**, 020407(R) (2013).
- [14] J. Klinovaja, P. Stano, A. Yazdani, and D. Loss, *Phys. Rev. Lett.* **111**, 186805 (2013).
- [15] B. Braunecker and P. Simon, *Phys. Rev. Lett.* **111**, 147202 (2013).
- [16] M. M. Vazifeh and M. Franz, *Phys. Rev. Lett.* **111**, 206802 (2013).
- [17] F. Pientka, L. I. Glazman, and F. von Oppen, *Phys. Rev. B* **88**, 155420 (2013).
- [18] F. Pientka, L. I. Glazman, and F. von Oppen, *Phys. Rev. B* **89**, 180505 (2014).
- [19] S. Nakosai, Y. Tanaka, and N. Nagaosa, *Phys. Rev. B* **88**, 180503 (2013).
- [20] K. Pöyhönen, A. Westström, J. Röntynen, and T. Ojanen, *Phys. Rev. B* **89**, 115109 (2014).
- [21] Y. Kim, M. Cheng, B. Bauer, R. M. Lutchyn, and S. Das Sarma, *Phys. Rev. B* **90**, 060401 (2014).
- [22] P. M. R. Brydon, S. Das Sarma, H.-Y. Hui, and J. D. Sau, *Phys. Rev. B* **91**, 064505 (2015).
- [23] H. Ebisu, K. Yada, H. Kasai, and Y. Tanaka, *Phys. Rev. B* **91**, 054518 (2015).
- [24] J. Li, H. Chen, I. K. Drozdov, A. Yazdani, B. A. Bernevig, and A. H. MacDonald, *Phys. Rev. B* **90**, 235433 (2014).
- [25] Y. Peng, F. Pientka, L. I. Glazman, and F. von Oppen, *Phys. Rev. Lett.* **114**, 106801 (2015).
- [26] A. Heimes, D. Mandler, and P. Kotetes, *New Journal of Physics* **17**, 023051 (2015).
- [27] A. Westström, K. Pöyhönen, and T. Ojanen, *Phys. Rev. B* **91**, 064502 (2015).
- [28] J. Zhang, Y. Kim, E. Rossi, and R. M. Lutchyn, *Phys. Rev. B* **93**, 024507 (2016).
- [29] S. Nadj-Perge, I. K. Drozdov, J. Li, H. Chen, S. Jeon, J. Seo, A. H. MacDonald, B. A. Bernevig, and A. Yazdani, *Science* (2014), 10.1126/science.1259327.
- [30] R. Pawlak, M. Kisiel, J. Klinovaja, T. Meier, S. Kawai, T. Glatzel, D. Loss, and E. Meyer, *ArXiv e-prints* (2015), [arXiv:1505.06078 \[physics.atm-clus\]](https://arxiv.org/abs/1505.06078).
- [31] L. Yu, *Acta Physica Sinica* **21**, 75 (1965).
- [32] H. Shiba, *Progress of Theoretical Physics* **40**, 435 (1968).
- [33] A. I. Rusinov, *Soviet Journal of Experimental and Theoretical Physics Letters* **9**, 85 (1969).
- [34] G. Moore and N. Read, *Nuclear Physics B* **360**, 362 (1991).
- [35] C. Nayak and F. Wilczek, *Nuclear Physics B* **479**, 529 (1996).
- [36] N. Read and D. Green, *Phys. Rev. B* **61**, 10267 (2000).
- [37] D. A. Ivanov, *Phys. Rev. Lett.* **86**, 268 (2001).
- [38] C. Nayak, S. H. Simon, A. Stern, M. Freedman, and S. Das Sarma, *Rev. Mod. Phys.* **80**, 1083 (2008).
- [39] J. Alicea, *Reports on Progress in Physics* **75**, 076501 (2012).
- [40] C. Beenakker, *Annual Review of Condensed Matter Physics* **4**, 113 (2013).
- [41] A. Y. Kitaev, *Physics-Uspekhi* **44**, 131 (2001).
- [42] A. Altland and M. R. Zirnbauer, *Phys. Rev. B* **55**, 1142 (1997).
- [43] A. P. Schnyder, S. Ryu, A. Furusaki, and A. W. W. Ludwig, *Phys. Rev. B* **78**, 195125 (2008).
- [44] A. Kitaev, in *American Institute of Physics Conference Series*, American Institute of Physics Conference Series, Vol. 1134, edited by V. Lebedev and M. Feigel'Man (2009) pp. 22–30.
- [45] G. Sharma and S. Tewari, *ArXiv e-prints* (2016), [arXiv:1603.08909 \[cond-mat.str-el\]](https://arxiv.org/abs/1603.08909).

Supplemental Material for “Topological Yu-Shiba-Rusinov chain in monolayer transition-metal dichalcogenide superconductors”

ANALYTICAL EXPRESSIONS OF INTEGRALS $I_0(\mathbf{r}, E)$ AND $I_1(\mathbf{r}, E)$

We provide the analytical expressions of the integral functions defined in Eqs. (5) and (6):

$$I_0(\mathbf{r}, E) = -\frac{\pi N_F}{\sqrt{\Delta^2 - E^2}} \text{Re} \left\{ J_0 \left[(k_F + i\xi_0^{-1}) r \right] + iH_0 \left[(k_F + i\xi_0^{-1}) r \right] \right\}, \quad (\text{S1})$$

$$I_1(\mathbf{r}, E) = -\pi N_F \text{Im} \left\{ J_0 \left[(k_F + i\xi_0^{-1}) r \right] + iH_0 \left[(k_F + i\xi_0^{-1}) r \right] \right\}, \quad (\text{S2})$$

where $r = |\mathbf{r}|$, $J_n(z)$ and $H_n(z)$ are Bessel and Struve functions of order n , respectively, and $\xi_0^{-1} \equiv \frac{\sqrt{\Delta^2 - E^2}}{-v_F}$, $v_F < 0$ for the valence bands. $\xi_0^{-1} \approx \frac{\Delta}{-v_F}$ corresponds to the inverse of superconducting coherence length in the host superconductor. Note that we take $\mathbf{r} \neq 0$ here.

ASYMPTOTIC FORMS FOR $I_0(\mathbf{r}, E)$ AND $I_1(\mathbf{r}, E)$

In order to perform Fourier transform of the Hamiltonian to momentum space, we use the asymptotic forms of the Bessel and Struve functions valid for large values of the argument close to the positive real axis. This is valid in our calculation because we consider shallow YSR band cases, i.e., the spacing between the adatoms is large $k_F a \gg 1$. In the limit $k_F r \gg 1$, we can find the approximate expressions for I_0 and I_1 , to the leading order, as

$$I_0(\mathbf{r}, E) = -\frac{\pi N_F}{\sqrt{\Delta^2 - E^2}} \sqrt{\frac{2}{\pi k_F r}} e^{-\xi_0^{-1} r} \cos \left[k_F r - \frac{1}{4} \pi \right], \quad (\text{S3})$$

$$I_1(\mathbf{r}, E) = -\pi N_F \sqrt{\frac{2}{\pi k_F r}} e^{-\xi_0^{-1} r} \sin \left[k_F r - \frac{1}{4} \pi \right]. \quad (\text{S4})$$

FOURIER TRANSFORMS OF $\mathcal{I}_0^\pm(\mathbf{r}, E)$ AND $\mathcal{I}_1^\pm(\mathbf{r}, E)$

The Fourier transforms of the effective Hamiltonian can be carried out analytically when utilizing the asymptotic expressions. For

$$\mathcal{I}_0^\pm(\mathbf{r}, E) = \frac{1}{3} \sum_n e^{\pm i \mathbf{K}_n \cdot \mathbf{r}} I_0(\mathbf{r}, E), \quad \mathcal{I}_1^\pm(\mathbf{r}, E) = \frac{1}{3} \sum_n e^{\pm i \mathbf{K}_n \cdot \mathbf{r}} I_1(\mathbf{r}, E), \quad (\text{S5})$$

define the Fourier transform as

$$f(p) = \sum_{j=-\infty}^{\infty} f(a_j) e^{i p a_j}.$$

Then the Fourier transforms of $\mathcal{I}_0^\pm(\mathbf{r})$ and $\mathcal{I}_1^\pm(\mathbf{r})$ to the momentum along the chain take the form,

$$\begin{aligned} \mathcal{I}_0^\pm(p, E) = & -\frac{\pi N_F}{\sqrt{\Delta^2 - E^2}} \sqrt{\frac{1}{2\pi k_F a}} \frac{1}{3} \sum_{n=0,1,2} \\ & \left\{ e^{-i\frac{\pi}{4}} \left[\text{Li}_{\frac{1}{2}} \left(e^{\pm i K a \cos(n\frac{2}{3}\pi + \varphi_c) + i k_F a + i p a - \xi_0^{-1} a} \right) + \text{Li}_{\frac{1}{2}} \left(e^{\mp i K a \cos(n\frac{2}{3}\pi + \varphi_c) + i k_F a - i p a - \xi_0^{-1} a} \right) \right] \right. \\ & \left. + e^{i\frac{\pi}{4}} \left[\text{Li}_{\frac{1}{2}} \left(e^{\pm i K a \cos(n\frac{2}{3}\pi + \varphi_c) - i k_F a + i p a - \xi_0^{-1} a} \right) + \text{Li}_{\frac{1}{2}} \left(e^{\mp i K a \cos(n\frac{2}{3}\pi + \varphi_c) - i k_F a - i p a - \xi_0^{-1} a} \right) \right] \right\}, \quad (\text{S6}) \end{aligned}$$

$$\begin{aligned}
\mathcal{I}_1^\pm(p, E) = & i\pi N_F \sqrt{\frac{1}{2\pi k_F a}} \frac{1}{3} \sum_{n=0,1,2} \\
& \left\{ e^{-i\frac{\pi}{4}} \left[\text{Li}_{\frac{1}{2}} \left(e^{\pm iKa \cos(n\frac{2}{3}\pi + \varphi_c) + ik_F a + ipa - \xi_0^{-1} a} \right) + \text{Li}_{\frac{1}{2}} \left(e^{\mp iKa \cos(n\frac{2}{3}\pi + \varphi_c) + ik_F a - ipa - \xi_0^{-1} a} \right) \right] \right. \\
& \left. - e^{i\frac{\pi}{4}} \left[\text{Li}_{\frac{1}{2}} \left(e^{\pm iKa \cos(n\frac{2}{3}\pi + \varphi_c) - ik_F a + ipa - \xi_0^{-1} a} \right) + \text{Li}_{\frac{1}{2}} \left(e^{\mp iKa \cos(n\frac{2}{3}\pi + \varphi_c) - ik_F a - ipa - \xi_0^{-1} a} \right) \right] \right\}, \quad (\text{S7})
\end{aligned}$$

where $\text{Li}_s(z)$ is the polylogarithm function:

$$\text{Li}_s(z) = \sum_{n=1}^{\infty} \frac{z^n}{n^s}.$$

EXPRESSIONS FOR \hat{M}_0 , \hat{M}_1 , AND $\hat{M}_{ij}(E \rightarrow 0)$

We provide the analytical expressions for \hat{M}_0 , \hat{M}_1 , and $\hat{M}_{ij}(E \rightarrow 0)$ in \hat{H}_{ij} of Eq. (16):

$$\hat{M}_0 = 1 - \tilde{J} \hat{\rho}_x \hat{\mathbf{S}}_i \cdot \hat{\boldsymbol{\sigma}}, \quad \hat{M}_1 = \frac{\tilde{J}}{\Delta} \left(\hat{\mathbf{S}}_i \cdot \hat{\boldsymbol{\sigma}} \right), \quad (\text{S8})$$

$$\begin{aligned}
\hat{M}_{ij}(E \rightarrow 0) = & \frac{1}{2} JS \left\{ [\mathcal{I}_1^+(\mathbf{R}_{ij}, 0) + \mathcal{I}_1^-(\mathbf{R}_{ij}, 0)] \hat{\rho}_z + \Delta [\mathcal{I}_0^+(\mathbf{R}_{ij}, 0) + \mathcal{I}_0^-(\mathbf{R}_{ij}, 0)] \hat{\rho}_x \right\} \left(\hat{\mathbf{S}}_j \cdot \hat{\boldsymbol{\sigma}} \right) \\
& + \frac{1}{2} JS \left\{ [\mathcal{I}_1^+(\mathbf{R}_{ij}, 0) - \mathcal{I}_1^-(\mathbf{R}_{ij}, 0)] \hat{\rho}_z + \Delta [\mathcal{I}_0^+(\mathbf{R}_{ij}, 0) - \mathcal{I}_0^-(\mathbf{R}_{ij}, 0)] \hat{\rho}_x \right\} \hat{\sigma}_z \left(\hat{\mathbf{S}}_j \cdot \hat{\boldsymbol{\sigma}} \right), \quad (\text{S9})
\end{aligned}$$

where $\hat{\mathbf{S}} \equiv \mathbf{S}/S$.